Contents lists available at ScienceDirect

Applied Catalysis B: Environmental

Research Paper

Efficient bimetallic NiCu-SiO$_2$ catalysts for selective hydrogenolysis of xylitol to ethylene glycol and propylene glycol

Hailong Liu [a], Zhiwei Huang [a,*], Haixiao Kang [a], Xuemei Li [a], Chungu Xia [a], Jing Chen [a,*], Haichao Liu [b]

[a] State Key Laboratory for Oxo Synthesis and Selective Oxidation, Suzhou Research Institute of LICP, Lanzhou Institute of Chemical Physics (LICP), Chinese Academy of Sciences, Lanzhou 730000, China
[b] Beijing National Laboratory for Molecular Sciences, College of Chemistry and Molecular Engineering, Peking University, Beijing 100871, China

ABSTRACT

The selective hydrogenolysis of biomass-derived xylitol to ethylene glycol and propylene glycol was carried out over non-noble Ni-decorated Cu-SiO$_2$ nanocatalysts with a wide range of Cu/Ni mass ratios and metal loadings in the presence of Ca(OH)$_2$. The NiCu-SiO$_2$ bimetallic catalysts showed much superior activities and selectivities to the target glycols relative to the monometallic Cu-SiO$_2$ and Ni-SiO$_2$ catalysts. Among them, 10Ni80Cu-SiO$_2$ catalyst (10/80 refers to the mass ratio of NiO and CuO) prepared by co-precipitation-gel method presented the highest activity and target glycols selectivity, and up to 81.0% combined glycol yield was attained at 473 K and 8 MPa H$_2$. Moreover, this catalyst exhibited greatly enhanced stability in repeated runs. Characterization of these catalysts by XRD, XPS, BET, N$_2$O-chemisorption, H$_2$-TPR and TEM showed that the decoration of suitable amount of Ni into Cu-SiO$_2$ catalysts had favorable effects on Cu dispersion, catalyst reducibility and the formation of highly active Ni surface-enriched Cu-Ni alloy sites. The notably enhanced performances of the NiCu-SiO$_2$ bimetallic catalysts could be ascribed to their significantly promoted C–OH dehydrogenation and C=O hydrogenation activities and high resistance to sintering of the active sites, imposed by the structural and electronic effects of Ni. Clearly, these findings provide useful guidance for the design of more efficient and stable non-noble bimetallic nanocatalysts for upgrading biomass-derived platform compounds particularly *via* hydrogenation/hydrogenolysis reactions.

© 2017 Elsevier B.V. All rights reserved.

1. Introduction

Due to the depletion of fossil resources and the growing concern over environmental problems, the transformation of abundant renewable biomass resources into liquid fuels and chemicals has attracted increasing attention in recent years [1–5]. Among biomass-based feedstocks, non-edible lignocellulose-derived xylitol and sorbitol are attractive platform chemicals which can be efficiently converted into various chemicals and biofuels, such as glycols [6–9], alkanes [10,11], aromatics [12] and cyclic ethers [13,14]. Glycols, including ethylene glycol and propylene glycol, in particular, are among the most versatile and important commodity chemicals in the world, with an estimated global demand exceeding 20 million metric tons in 2016 [15,16]. Currently, the

glycols are industrially produced by the multi-step transformations of non-renewable petroleum-derived ethylene and propylene *via* their epoxides. Ready availability from abundant lignocellulose and structural analogy to glycols with adjacent hydroxyl groups render xylitol and sorbitol to be the ideal feedstocks for the sustainable synthesis of the two glycols by catalytic hydrogenolysis with high energy efficiency [7].

The hydrogenolysis of xylitol and sorbitol to target glycols requires selective cleavage of C–C and C–O bonds. So far, both noble metals (*e.g.* Ru [7,17–22], Pd [7,23], Pt [24]) and base metals (*e.g.* Ni [6,8,25–27], Cu [9,28,29]) have been studied for the hydrogenolysis of sugar alcohols to glycols (Table 1), generally with the promotion of basic additives (*e.g.* CaO, Ca(OH)$_2$, NaOH). Due to their high activity for C–C bond cleavage, Ni- and Ru- based catalysts have been frequently applied for sugar alcohols hydrogenolysis at 473–513 K and 4–8 MPa H$_2$ [6–8,17–22,25–27]. Unfortunately, these catalysts can also catalyze the excessive C–C bond scission to form large amount of byproducts (*e.g.* methane) [7,8,30,31], and thus resulting in unsatisfactory yields to the target glycols (<70% in most

Table 1
Some typical results for the selective hydrogenolysis of sugar alcohols.

Catalyst	Subtract	Promoter	Reaction condition			Conversion (%)	Yield (%)		Ref.
			T (K)	P (MPa)	Time (h)		Ethylene glycol	Propylene glycol	
Ru/CNF	Sorbitol	CaO	493	8	1	91.8	17.2	30.8	[21]
RuWO$_x$/CNTs	Sorbitol	Ca(OH)$_2$	478	5	2	99.6	25.6	34.6	[17]
NiPt/NaY	Sorbitol	/	493	6	6	59	5.9	42.5	[24]
Ni/NaY	Sorbitol	Ca(OH)$_2$	493	6	6	75	5.2	51.8	[24]
NiCe/Al$_2$O$_3$	Sorbitol	Ca(OH)$_2$	513	7	8	91.1	16.3	32.1	[8]
NiRuCa	Sorbitol	Ca(OH)$_2$	493	4	4	93.6	14.5	31.8	[19]
Ni-Re/C	Sorbitol	Ba(OH)$_2$	523	1 (N$_2$)	0.5	91.7	14.5	28.4	[27]
Ni/MgO	Sorbitol	/	473	4	4	67.8	17.6	22.8	[25]
PdCu/ZrO$_2$	Sorbitol	La(OH)$_3$	493	5	4	100	15.9	37.0	[23]
Ru/C	Sorbitol	Ca(OH)$_2$	473	4	2	98.0	26.5	32.1	[37]
Ru/C	Xylitol	Ca(OH)$_2$	473	4	6	98.0	32.3	27.8	[7]
Ni$_2$P/AC	Xylitol	Ba(OH)$_2$	473	4	0.75	98.6	17.0	27.7	[38]
Ni-CaO/C	Xylitol	/	473	4	2	~100	28.4	26.0	[26]
Cu/CaO-Al$_2$O$_3$	Xylitol	/	503	2.8	10	98.9	25.7	43.9	[29]
Cu/CaO-Al$_2$O$_3$	Sorbitol	/	503	7	4	98.1	15.1	45.2	[29]
Cu-SiO$_2$	Xylitol	Ca(OH)$_2$	473	6	2	>99	32.8	37.6	[28]
NiCu-SiO$_2$	Xylitol	Ca(OH)$_2$	473	8	1	~100	38.5	42.5	This work

cases, Table 1). Differently, Cu is known for its high efficiency in C–O bond hydro-dehydrogenation and poor reactivity for C–C bond cleavage [30–32]. Such properties render Cu-based catalysts to be favorable catalysts for glycerol hydrogenolysis to propylene glycol with selectivity up to above 97% [33–35]. Recent studies by Chaudhari et al. [29] and our groups [7,9,23,28,36,37] show that Cu catalysts also exhibited high yields in the hydrogenolysis of polyols to glycols, and a high combined yield of 70.4% to ethylene glycol and propylene glycol was attained over a uniformly dispersed Cu-SiO$_2$ catalyst prepared by precipitation-gel method in xylitol hydrogenolysis [28]. Notwithstanding these efforts, it is still a great challenge to achieve high glycol yields (e.g. above 80%) in sugar alcohols hydrogenolysis at mild conditions, probably due to the high reactivity of both the reactants and their carbonyl intermediates during the reaction.

It is widely accepted that hydrogenolysis of C$_5$ and C$_6$ polyols to ethylene glycol and propylene glycol involves three key steps (Scheme 1), i.e. kinetically relevant dehydrogenation of C$_5$ and C$_6$ polyols to the corresponding C$_5$ or C$_6$ sugar intermediates on metal surfaces; subsequently, C–C bond cleavage of these intermediates catalyzed by base promoters via the retro-aldol condensation, and the hydrogenation of the carbonyl intermediates from the retro-aldol condensation to the target glycols on metal surfaces [7,18,29,37,39,40]. Clearly, the hydrogenolysis rate is governed by the dehydrogenation activity of metal surface. Nonetheless, the final glycol selectivity is also determined by the hydrogenation activity of metal catalyst, since the hydrogenation of the carbonyl intermediates from the retro-aldol condensation and their base-catalyzed side reactions to form acid byproducts are competitive reactions [7,9,26]. Thus, in the presence of sufficient base promoter, the enhancement in dehydrogenation activity of metal surface would benefit the reaction rate of C$_5$ and C$_6$ polyol hydrogenolysis, while enhancement in hydrogenation activity of metal surface would increase the glycol selectivity.

Recently, supported bimetallic catalysts have gained considerable attention due to their enhanced catalytic activities, selectivities and stability, compared with their monometallic counterparts [2,41,42]. As an example, Cu-Ni bimetallic catalysts have been widely applied in many important reactions, such as synthesis of methanol and higher alcohols [43–45], hydrogenation of esters and furfurals [46–48], dehydrogenation of alcohols and organic hydrides [49,50], and steam reforming of alcohols and tars [51,52]. Despite several bimetallic catalysts have been attempted for the selective hydrogenolysis of sugar alcohols (Table 1), such studies on non-noble Ni-Cu bimetallic catalysts are still rare so far [2–4].

Although Cu metal is effective for C–O hydro-dehydrogenation as mentioned above, it is not very active for H$_2$ activation [31], likely due to its lower binding energy to hydrogen (−2.39 eV) in comparison with other transition metals such as Ni and Co with much stronger binding (−2.89 eV) [53]. As a result, Cu catalysts generally present inferior activities for C=O and C=C bond hydrogenation in comparison with Ni and Co catalysts [54,55]. For these reasons, the decoration of Cu nanoparticles by a second metal like Ni with high H$_2$ activation capability can be an effective strategy to combine high selectivity of Cu metal and high hydrogenation capacity of the metal promoter, which would result in an efficient bimetallic catalyst for sugar alcohols hydrogenolysis.

In the present work, a series of NiCu-SiO$_2$ bimetallic catalysts with different Cu/Ni mass ratios and different metal loadings were prepared by a co-precipitation-gel (CPG) method and tested in the hydrogenolysis of xylitol to ethylene glycol and propylene glycol. For comparison, the structural and catalytic performances of monometallic Cu and Ni catalysts with different metal loadings prepared by precipitation-gel (PG) method as well as a 10Ni/80Cu-SiO$_2$ bimetallic catalyst prepared by impregnation (IM) of Ni onto 80Cu-SiO$_2$ were also studied. The NiCu-SiO$_2$ bimetallic catalysts were found to present much superior performances (including activity, selectivity and stability) than those of their monometallic counterparts, and a high combined yield of ethylene glycol and propylene glycol up to 81% was attained over an efficient 10Ni80Cu-SiO$_2$ catalyst. The detailed structure-activity relationship of the Ni-Cu bimetallic catalysts in xylitol hydrogenolysis was studied, and possible reasons for the enhanced performances of the bimetallic catalysts were also discussed.

2. Experimental

2.1. Catalyst preparation

The Cu-SiO$_2$ and Ni-SiO$_2$ monometallic samples with metal oxide loadings from 10 to 90 wt% were prepared by precipitation-gel (PG) method as described in our previous reports [28,33]. Colloidal aqueous solution of SiO$_2$ (25.0 wt%, ammonium stabilized type, pH ~ 8.5–10.5, particle sizes 10–20 nm) was purchased from Qingdao Haiyang Chemical Co., China. NiCu-SiO$_2$ bimetallic catalysts with different CuO/NiO mass ratio and different metal oxide loadings were prepared by co-precipitation-gel (CPG) method with the mixture solution of Cu(NO$_3$)$_2$ (0.5 mol/L) and Ni(NO$_3$)$_2$ co-precipitated with NaOH (4 mol/L) at a constant rate. Other procedures were the same as PG method. The calcined samples were
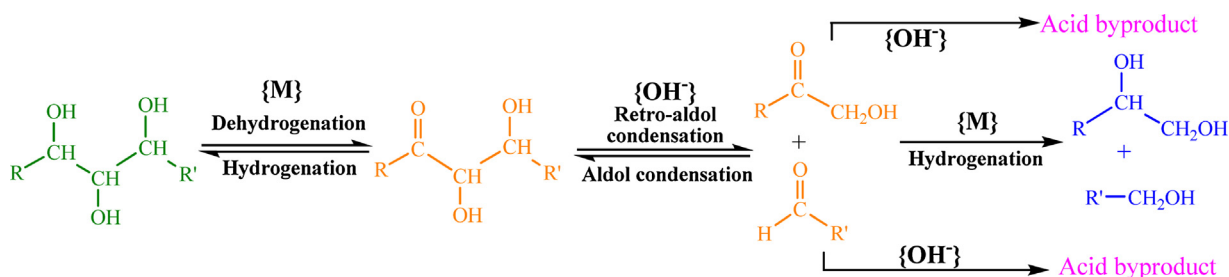
Scheme 1. General reaction pathways for hydrogenolysis of C_5 and C_6 polyols to glycols and also acid byproducts.

marked as xNiOyCuO-SiO$_2$, and the corresponding reduced catalysts were marked as xNiyCu-SiO$_2$, where x and y represents the nominal mass loading of NiO and CuO (wt%), respectively. For comparison, unsupported Cu and Ni catalysts (named pure Cu and pure Ni, respectively) were prepared by precipitating the Cu(NO$_3$)$_2$ (0.5 mol/L) or Ni(NO$_3$)$_2$ (0.5 mol/L) aqueous solution with NaOH (4 mol/L), respectively, and the other treatments were similar as above. The 10Ni/80Cu-SiO$_2$ and 10Ni/SiO$_2$ catalysts were prepared by incipient wetness impregnation (IM) method. The calcined 80CuO-SiO$_2$ sample (prepared by PG method) and SiO$_2$ support (purchased from Alfa Aesar, surface area: 360–410 m^2/g) were separately impregnated with an aqueous solution containing the calculated amount of Ni(NO$_3$)$_2$ at room temperature, followed by drying at 393 K overnight and calcining at 723 K for 3 h in air.

2.2. Catalyst characterization

The X-ray powder diffraction (XRD) was performed with a PANalyticalX'pert Pro Diffractometer using Cu Ka radiation (λ = 1.54178 Å). The *in situ* XRD measurements were also carried out on this instrument equipped with a XRK-900 high-temperature chamber. The XRD patterns were obtained after *in situ* reduction in 5%H$_2$-Ar at a flow rate of 50 mL/min up to 573 or 723 K for selected Cu-containing or monometallic Ni samples, respectively. In these experiments, the temperature was ramped at a heating rate of 10 K/min to the target temperature and maintained at this temperature for 2 h before recording the pattern. The crystallite sizes (d) of metal oxides or metals in the samples were calculated by the Scherrer equation $d = k\lambda/\beta_L \cos\theta$ [56], where k is the Debye-Scherrer constant (0.89), θ is the Bragg angle, and β_L is the half-width of the diffraction peak. The compositions of the Ni-Cu alloy particles in terms of Cu^0/Ni^0 ratio were estimated by the Vegard's law (d_{CuNi} = Ni/(Ni + Cu) × d_{Ni} + Cu/(Ni + Cu) × d_{Cu}), where d_{Cu} and d_{Ni} from the d(111) spacing from XRD are 0.2088 nm (JCPDS 04-0836) and 0.2034 nm (JCPDS 04-0850), respectively.

X-ray photoelectron spectra (XPS) measurements were carried out on an ESCALAB250xi spectrometer equipped with an Al Ka X-ray radiation source (hν = 1486.6 eV). The spectra were recorded with constant pass energy of 20 eV, and the binding energies were calibrated using the Si2p peak at 103.4 eV as the reference. For the *in situ* experiments, the selected Cu-containing and monometallic Ni samples were reduced in a pretreatment chamber at 573 or 723 K for 2 h with 20% H$_2$–N$_2$ at a flow rate of 50 mL/min, respectively. After cooling to room temperature, the pretreatment chamber was evacuated to 10^{-3} Pa, and then the reduced catalysts were transferred to analytic chamber for XPS measurement without exposure to air.

The BET surface area and pore structures were measured by N$_2$ adsorption–desorption experiments on a Micromeritics Tristar II 3020 instrument at 77 K after pretreatment in N$_2$ flow at 573 K for 3 h. Transmission electron microscopic (TEM) investigations were performed on a JEM2010 electron microscope. The practical Cu and Ni loadings in different samples were detected using an

atomic absorption spectrometer (AAS, Analytik Jena ContrAA 700) at 249.2 nm.

The reducibility of the calcined catalyst precursors was characterized by hydrogen temperature programmed reduction (H$_2$-TPR), while the Cu dispersion was determined by dissociative N$_2$O adsorption–H$_2$-TPR reverse titration [28,57]. Both types of assays were carried out using a unit DAX-7000 instrument (Huasi Technology Co., Ltd, China). For H$_2$-TPR experiments, the samples containing $\sim$10 mg Cu were placed in a quartz cell and pretreated at 473 K under He flow for 1 h. Then after cooling to 303 K, they were reduced with a 5%H$_2$-Ar flow (40 mL/min), and the temperature increased linearly to 773 K at a ramping rate of 5 K/min. The H$_2$ consumption was monitored by a thermal conductivity detector (TCD). For determining Cu dispersion, the calcined samples were firstly reduced by the same H$_2$-TPR procedure described above (denoted as total TPR). After cooling to 323 K, the reduced samples were exposed to a 5%N$_2$O–N$_2$ flow (40 mL/min, 1 h) for mild oxidation of the surface Cu^0 to Cu$_2$O. Afterwards, the resulting surface oxidized samples underwent the second TPR run as the first one (denoted as surface TPR). The Cu dispersion (D_{Cu}), specific exposed Cu surface area (S_{Cu}) and average Cu particle size (d_{Cu}) were calculated by Eqs. (1)–(3), respectively, by assuming a spherical shape of the copper metal particles and 1.46 × 10^{19} Cu atoms per m^2 [57].

$$D_{Cu}(\%) = \frac{2 \times H_2 \text{ Consumption (surface TPR)}}{H_2 \text{ Consumption (total TPR)}} \times 100 \quad (1)$$

$$S_{Cu}(\text{m}^2\text{g}^{-1}\text{Cu}) = \frac{D_{Cu} \times N_{av}}{M_{Cu} \times 1.46 \times 10^{19}} \approx 649 \times D_{Cu} \quad (2)$$

$$d_{Cu}(\text{nm}) = \frac{6}{S_{Cu} \times \rho_{Cu}} \approx \frac{1.0}{D_{Cu}} \quad (3)$$

Where N_{av}: Avogadro constant = 6.02 × 10^{23} (mol^{-1}); M_{Cu}: relative atomic mass = 63.55 (g/mol); ρ_{Cu} Cu density = 8.92 (g/mL).

2.3. Catalytic testing

Xylitol hydrogenolysis reactions were carried out in a stainless steel autoclave (100 mL) at a stirring speed of 800 rpm. Prior to the reaction test, the Cu-containing samples were pre-reduced at 573 K in 20% H$_2$-–N$_2$ for 3 h, while monometallic Ni samples were reduced at 723 K to obtain the active catalysts. In a typical run, 40 g of 10 wt% xylitol ($\geq$99%, Alfa Aesar) aqueous solution, 0.144 g metal for the reduced catalyst and 0.600 g Ca(OH)$_2$ were introduced into the autoclave. After flushing with H$_2$ for 3 times, the autoclave was pressurized with H$_2$ and heated to the reaction temperature. The reactant and liquid products were silanized with hexamethyldisilazane (HMDS) and trimethylchlorosilane (TMSC) (both $\geq$98.0%, Alfa Aesar) in pyridine (AR, Xilong Chemical Co. Ltd, China) before analyzed by gas chromatograph (Agilent 7820A GC) with a SE-54 capillary column (50 m × 0.25 mm × 0.25 μm) and a flame ionization detector (FID). The conversion of xylitol and selectivity of products were calculated on a carbon basis as reported in our previous work [9].

The dehydrogenation of 1-pentanol and propylene glycol and the hydrogenation of xylose and acetol were also carried out in the 100 mL stainless steel autoclave with similar procedure as xylitol hydrogenolysis. For 1-pentanol and propylene glycol dehydrogenation, the autoclave was flushed and pressurized with N_2 to 3 MPa, then heated to 473 K. For xylose and acetol hydrogenation, the reactions were carried out at 6 MPa H_2 and 353 K. The reactant and liquid products were analyzed by the same GC for xylitol hydrogenolysis. Catalyst amount and reaction time were varied for the control of reaction conversion.

3. Results

3.1. Catalytic performances of silica-stabilized Cu, Ni and NiCu catalysts in xylitol hydrogenolysis

Table 2 shows the conversions and selectivities of Cu-SiO$_2$, Ni-SiO$_2$ and NiCu-SiO$_2$ catalysts with different metal loadings prepared by PG or CPG methods in xylitol hydrogenolysis at reaction conditions of 473 K and 6 MPa H_2. As can be seen, both monometallic Cu (entries 1–4) and Ni (entries 5–8) catalysts were active and selective in xylitol hydrogenolysis, and at a given amount of metal, their xylitol conversions and glycol selectivities increased with increasing metal loadings and reached maximum values at ~90 wt% metal loading. Such finding is probably due to the structure-sensitive nature of xylitol hydrogenolysis reaction, with the catalysts containing ~90 wt% metal loading possessed optimum metal particle size [9,28]. It appears that Cu-SiO$_2$ catalysts are superior to Ni-SiO$_2$ catalysts in xylitol hydrogenolysis, probably due to that Ni^0 had stronger adsorption capacities than Cu^0 for reactant and/or the carbonyl reaction intermediates. The strong interaction of Ni and reactant and/or reaction intermediates may limit the availability of active sites for the activation of other reactants or reaction intermediates, thus leading to some poisoning effects on the Ni^0 surface [46,58]. Nonetheless, the activities and selectivities of the Cu-SiO$_2$ catalysts are still unsatisfactory and need further improvement. To our delight, remarkable enhancements in both xylitol conversions and glycol selectivities were observed over the Ni-decorated Cu-SiO$_2$ catalysts (entries 9–11), as compared to those of the monometallic counterparts of Cu-SiO$_2$ (entries 1–3) and Ni-SiO$_2$ (entries 5–7) catalysts with the same metal loadings. Notably, a high xylitol conversion of 94.4% and selectivity of 28.8 and 31.6% respectively to ethylene glycol and propylene glycol were obtained over 10Ni80Cu-SiO$_2$ catalyst at such unoptimized reaction conditions, showing the promising potential of Ni-Cu bimetallic catalysts for polyol hydrogenolysis.

In addition, the effect of Ni loading with fixed metal oxides amount (90 wt%, entries 11–15 in Table 2) on xylitol hydrogenolysis was also studied to optimize the catalyst composition. The xylitol conversion increased sharply from 63.0% over 90Cu-SiO$_2$ without Ni decoration (Table 2, entry 3) to 94.4% over 10Ni80Cu-SiO$_2$ catalyst with 8 wt% Ni loading, and then decreased to 66.4% over 30Ni60Cu-SiO$_2$ catalyst with further increasing Ni loading to 25 wt%. Simultaneously, the combined selectivities to ethylene glycol and propylene glycol increased gradually from 55.4% on 90Cu-SiO$_2$ to a maximum value of 60.4% on 10Ni80Cu-SiO$_2$ catalyst and then declined to 43.3% on 30Ni60Cu-SiO$_2$ catalyst. The combined glycols yield increased steadily from 34.9% on 90Cu-SiO$_2$, reached a maximum of 57.0% on 10Ni80Cu-SiO$_2$ and then decreased to 28.8% on 30Ni60Cu-SiO$_2$ catalysts. These results show that 80/10 (wt%) is the optimum CuO: NiO mass ratio for NiCu-SiO$_2$ bimetallic catalysts in xylitol hydrogenolysis, which is probably due to that this catalyst possessed optimum and balanced C–OH dehydrogenation and C=O hydrogenation activities. It is likely that higher amounts of Cu is insufficient for the hydrogenation of the
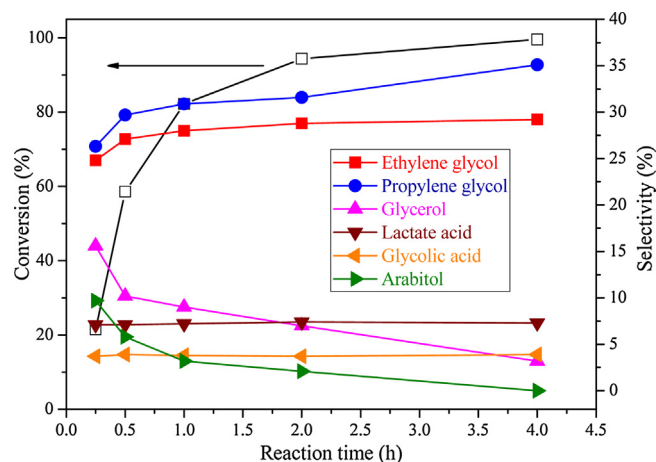

Fig. 1. Effect of reaction time on conversions and selectivities for xylitol hydrogenolysis on 10Ni80Cu-SiO$_2$ catalyst.
Reaction conditions: 40 g 10 wt% xylitol aqueous solution, 0.144 g active metal, 0.600 g Ca(OH)$_2$, 473 K, 6 MPa H_2.

C=O bonds in carbonyl intermediates (leading to larger amount of acid byproducts, *e.g.* on 90 Cu-SiO$_2$), while higher loadings of Ni lead to lower C–OH dehydrogenation activity and excessive C–C bond scission (showing a lower activity, selectivity and carbon balance, as observed on 30Ni60Cu-SiO$_2$). Therefore, the catalyst having a proper Cu/Ni ratio presented the highest activity and glycols selectivity in xylitol hydrogenolysis.

To examine the intrinsic properties of Ni-decorated Cu-SiO$_2$ catalysts, the activities and selectivities for representative silica-stabilized monometallic Cu and Ni catalysts and bimetallic Ni-Cu catalysts in xylitol hydrogenolysis were investigated at 473 K and 6 MPa H_2 at similar xylitol conversions (~30%) within kinetic-controlled regime. As shown in Table 3, the xylitol hydrogenolysis activity, defined as the mole of converted xylitol per mole of metal per hour, was 59.3 h^{-1} on 10Ni80Cu-SiO$_2$, about 6, 7 and 300 times higher than these on 90Cu-SiO$_2$, 80Cu-SiO$_2$ and 10Ni-SiO$_2$ catalysts (prepared by PG method), respectively. Concurrently, the selectivity to ethylene glycol and propylene glycol on 10Ni80Cu-SiO$_2$ was also superior to these obtained on 90Cu-SiO$_2$, 80Cu-SiO$_2$ and 10Ni-SiO$_2$ catalysts. In addition, a high activity of 17.1 h^{-1} was also achieved on 10Ni/80Cu-SiO$_2$ catalyst prepared by impregnating Ni on the calcined 80CuO-SiO$_2$ sample, which was about 1.7, 2 and 8 times higher than that on 90Cu-SiO$_2$, 80Cu-SiO$_2$ prepared by PG method and 10Ni/SiO$_2$ catalyst prepared by IM method, respectively. Similar to 10Ni80Cu-SiO$_2$, the selectivity to ethylene glycol and propylene glycol on 10Ni/80Cu-SiO$_2$ was also superior to these obtained on 90Cu-SiO$_2$, 80Cu-SiO$_2$ and 10Ni/SiO$_2$. Such findings demonstrate the remarkable promotion effect of Ni on Cu-containing catalyst in xylitol hydrogenolysis. The much higher activity (~3 times) for 10Ni80Cu-SiO$_2$, relative to 10Ni/80Cu-SiO$_2$, can be ascribed to its higher dispersion of Ni and more intimate interaction of Cu with Ni, as discussed below.

The reaction parameters, including temperature, H_2 pressure, substrate concentration (Table 4) and time (Fig. 1), were optimized to achieve high yields of ethylene glycol and propylene glycol in xylitol hydrogenolysis. Both the conversions of xylitol and the selectivities to the target glycols decreased with increasing xylitol concentration (2.5–20 wt%) at fixed catalyst amount, suggesting that high ratio of metal catalyst to substrate favors not only the conversion of xylitol but also the selectivity to the target glycols under sufficient amount of base promoter, which is in line with previous findings [7,21,28,37]. Both xylitol conversions and glycols selectivities increased with increasing H_2 pressure in the range of 4–8 MPa, while the optimal xylitol conversion and glycols selec-

Table 2

Conversions and selectivities of Cu-SiO₂, Ni-SiO₂ and NiCu-SiO₂ catalysts with different metal loadings in xylitol hydrogenolysis.[a]

Entry	Catalyst	Conversion (%)	Selectivity (%)								
			Ethylene glycol	Propylene glycol	Glycerol	Lactate acid	Glycolic acid	Arabitol	Dehydrated products[b]	Others[d]
1	10Cu-SiO₂	6.4	11.8	9.3	3.1	17.8	8.8	13.3	1.0	34.9
2	50Cu-SiO₂	55.0	19.8	20.5	4.8	16.0	6.4	10.1	5.2	17.2
3	90Cu-SiO₂	63.0	26.1	29.3	7.2	10.2	4.8	10.6	4.6	7.2
4	Pure Cu	39.7	19.9	18.2	6.2	14.1	7.2	18.1	4.9	11.4
5	10Ni-SiO₂	5.6	3.5	2.2	1.5	20.1	11.0	3.9	0.6	57.2
6	50Ni-SiO₂	23.6	24.9	21.0	1.6	17.5	9.1	4.4	1.9	19.6
7	90Ni-SiO₂	41.5	28.1	27.0	8.6	4.6	1.1	7.7	6.2	16.7
8	Pure Ni	15.1	12.7	15.6	4.8	15.8	8.7	11.1	5.4	25.9
9	1·1Ni8·9Cu-SiO₂[c]	11.7	13.1	10.0	3.5	17.8	8.4	17.4	1.6	28.2
10	5·6Ni44·4Cu-SiO₂[c]	62.9	24.7	24.2	7.4	10.1	4.7	8.3	6.1	14.5
11	10Ni80Cu-SiO₂[c]	94.4	28.8	31.6	7.0	7.4	3.7	2.1	6.2	13.2
12	3Ni87Cu-SiO₂	71.7	26.7	29.9	7.8	9.0	4.2	10.3	5.1	7.0
13	5Ni85Cu-SiO₂	89.6	27.5	30.0	8.0	8.3	4.0	6.4	5.9	9.9
14	15Ni75Cu-SiO₂	84.4	26.4	27.9	8.9	8.3	4.1	7.8	4.0	12.6
15	30Ni60Cu-SiO₂	66.4	23.1	20.2	7.8	9.2	3.2	10.3	5.4	20.8

[a] Reaction conditions: 40 g 10 wt% xylitol aqueous solution, 0.144 g active metal, 0.600 g Ca(OH)₂, 473 K, 6 MPa H₂, 2 h.
[b] Consisting of 1,2,5-pentanetriols and 1,2,4,5-pentanetetrols.
[c] The CuO: NiO mass ratios were ~8: 1.
[d] Others including small amounts of methanol, formic acid, acetic acid, gas products (CO₂ and methane) and undetermined products.

Table 3

Catalytic performances of representative silica-stabilized monometallic Cu and Ni and bimetallic Ni-Cu catalysts in xylitol hydrogenolysis.[a]

| Catalyst	Conversion (%)	Catalyst amount (g)/Reaction time (h)	Activity (h⁻¹)[b]	Selectivity (%)							
				Ethylene glycol	Propylene glycol	Glycerol	Lactate acid	Glycolic acid	Arabitol	Dehydrated products[c]	Others[d]
10Ni-SiO₂	25.6	2.000/12	0.2	8.5	10.2	3.5	40.1	21.0	3.9	0.6	12.2
10Ni/SiO₂	30.9	1.500/2	2.2	12.9	15.1	6.8	23.2	13.4	10.9	1.4	16.3
80Cu-SiO₂	31.4	0.050/2	8.2	26.1	27.2	8.8	11.3	6.0	13.5	1.9	5.2
90Cu-SiO₂	30.2	0.034/2	10.3	27.4	28.0	9.7	10.8	5.7	15.4	2.2	0.8
10Ni80Cu-SiO₂	31.9	0.025/0.5	59.3	28.1	30.9	8.1	7.5	3.9	16.1	3.5	1.9
10Ni/80Cu-SiO₂	29.4	0.050/1	17.1	27.8	29.1	8.9	8.7	4.7	15.8	2.4	2.6

[a] Reaction conditions: 473 K, 6 MPa H₂, 40 g 10 wt% xylitol aqueous solution, 0.600 g Ca(OH)₂, ~30% conversion.
[b] Activity is defined as: the mole of converted xylitol per mol of metal per hour.
[c] Consisting of 1,2,5-pentanetriols and 1,2,4,5-pentanetetrols.
[d] Others including small amounts of methanol, formic acid, acetic acid, gas products (CO₂ and methane) and undetermined products.

Table 4

The effect of reaction parameters on xylitol hydrogenolysis over 10Ni80Cu-SiO₂ catalyst.[a]

Reaction conditions			Conversion (%)	Selectivity (%)							
Temperature (K)	Pressure (MPa)	Concentration (wt%)		Ethylene glycol	Propylene glycol	Glycerol	Lactate acid	Glycolic acid	Arabitol	Dehydrated products[b]	Others[c]
473	6	2.5	>99	35.0	38.4	4.4	3.6	2.4	0.2	9.3	6.7
473	6	5	97.6	33.2	37.6	6.1	4.3	2.7	0.3	5.8	10.0
473	6	10	94.4	28.8	31.6	7.0	7.4	3.7	2.1	6.2	13.2
473	6	20	76.2	27.1	27.4	5.4	6.3	3.1	7.7	5.4	17.6
453	6	10	69.4	28.5	25.5	10.1	3.0	1.2	8.9	7.9	14.9
493	6	10	90.7	28.7	30.2	6.2	6.0	2.6	3.1	5.8	17.4
473	4	10	88.0	23.3	24.2	6.4	9.2	4.6	3.4	5.7	23.2
473	8	10	97.4	29.5	34.5	7.4	4.3	2.0	1.5	7.0	13.8
473[d]	8	10	~100	38.5	42.5	4.1	3.0	1.4	–	8.1	2.4

[a] Reaction conditions: 40 g xylitol aqueous solution, 0.144 g active metal, 0.600 g Ca(OH)₂, 2 h.
[b] Consisting of 1,2,5-pentanetriols and 1,2,4,5-pentanetetrols.
[c] Others including small amounts of methanol, formic acid, acetic acid, gas products (CO₂ and methane) and undetermined products.
[d] Reaction conditions: 40 g xylitol aqueous solution, 0.576 g active metal, 0.600 g Ca(OH)₂, 1 h.

tivity was achieved at 473 K reaction temperature (Table 4). The slight decrease of xylitol conversion at a higher temperature of 493 K would be aroused by the deactivation of the catalyst due to structure change and surface coking under extreme high-basicity hydrothermal conditions [28]. The xylitol conversion rose sharply to 82.2% in the first 1 h, and then increased gently to 99.6% with the further increase of reaction time to 4 h. The selectivities to ethylene glycol and propylene glycol increased quickly to 28 and 30.9% after 1 h reaction and ascended slightly to 29.2 and 35.1% with increasing reaction time to 4 h, respectively (Fig. 1). The selectivities to glycerol and arabitol declined monotonously with rising reaction time, while the selectivities to acid byproducts (lactate acid and glycolic acid) kept almost constant during the reaction process, suggesting that glycerol and arabitol are reaction intermediates that
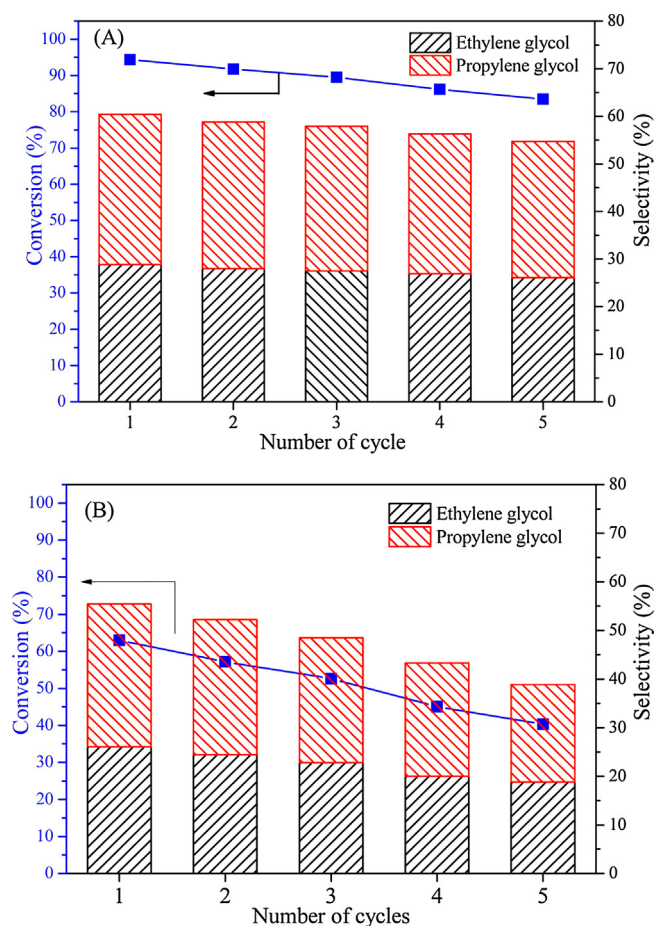
Fig. 2. Reusability results of xylitol hydrogenolysis on (A) 10Ni80Cu-SiO₂, (B) 90Cu-SiO₂ catalyst.

Reaction conditions: 40 g 10 wt% xylitol aqueous solution, 0.144 g metal, 0.600 g Ca(OH)₂, 473 K, 6 MPa H₂, 2 h. The collected catalyst was calcined in air at 723 K and reduced under H₂ atmosphere at 573 K for 3 h before further testing.

can be further converted mainly to the target glycol products as reported previously [7,9]. Therefore, these findings show that high yield of glycols could be achieved at proper catalyst to reactant ratio and optimum reaction temperature, H₂ pressure and reaction time. For instance, a much high combined ethylene glycol (38.5%) and propylene glycol (42.5%) yield (in total 81.0%) at full xylitol conversion was achieved over 10Ni80Cu-SiO₂ at 473 K and 8 MPa H₂ for 1 h in the hydrogenolysis of 10 wt% xylitol aqueous solution with 0.576 g active metal (Table 4), which is, to our knowledge, much higher than even most noble metal catalysts reported earlier for the hydrogenolysis of sugar and sugar alcohols.

The recyclability of the efficient 10Ni80Cu-SiO₂ was also studied and compared to its monometallic counterpart of 90Cu-SiO₂ with the same metal loading (Fig. 2). Previously, we found that re-calcination and reduction treatments were effective methods to reactivate the spent Cu-SiO₂ catalyst for xylitol hydrogenolysis by the simultaneous re-dispersion of Cu and the decomposition of coke [28]. Thus, the collected catalyst was re-calcined in air at 723 K and re-reduced with 20% H₂–N₂ at 573 K for 3 h before recharged into the autoclave together with fresh reactant and Ca(OH)₂ promoter. Only a slight decrease of xylitol conversion (from 94.4 to 83.5%) was seen on 10Ni80Cu-SiO₂ after 5 runs, meanwhile, the combined selectivity to ethylene glycol and propylene glycol declined from 60.4 to 54.7% (Fig. 2A). In contrast, the xylitol conversion and combined selectivity to the target glycols over 90Cu-SiO₂ catalyst descended sharply from 63.0 and 55.4% to 40.3 and 38.9%
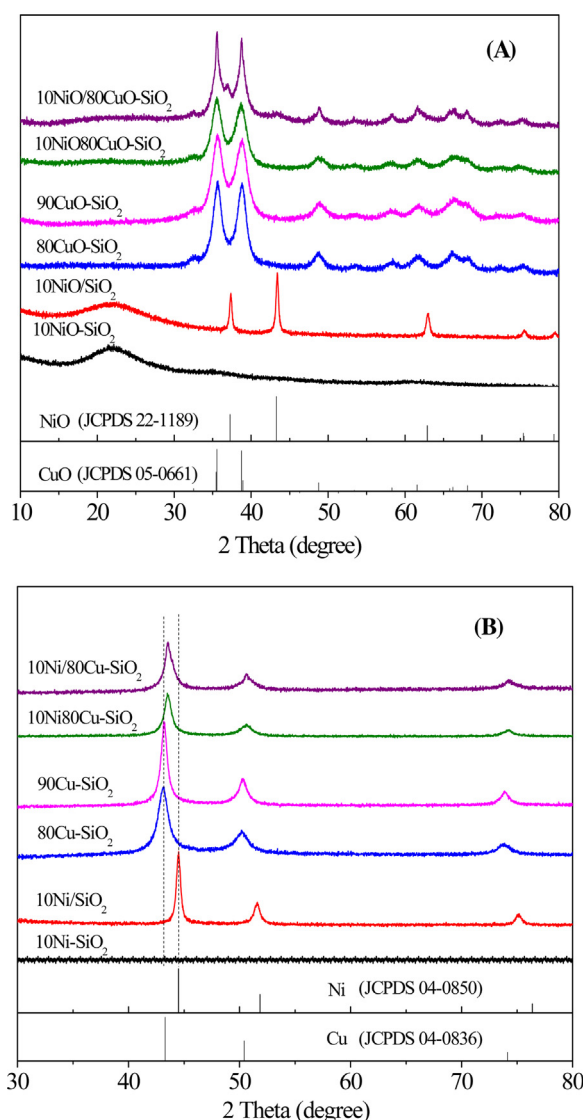
Fig. 3. XRD patterns of the representative silica-stabilized Cu, Ni and NiCu bimetallic catalysts after calcination (A) and *in situ* reduction in H₂ at 573 K (B).

after 5 cycles (Fig. 2B), respectively. Such comparison shows the remarkable increase in stability of Cu-SiO₂ catalyst by the decoration of Ni. Since the leaching of both Cu and Ni in the reaction media as detected by ICP were negligible (both <0.6 ppm), the main reasons for the gradual deactivation of the catalysts are inferred to the sintering of active metal/alloy particles and coke formation, as discussed below.

3.2. Structural characterizations of silica-stabilized Cu, Ni and Ni-Cu bimetallic catalysts

Fig. 3A shows the XRD patterns of the calcined representative silica-stabilized Cu, Ni and Ni-decorated Cu samples. The board diffraction peaks at $2\theta = \sim 22°$ in the 10NiO/SiO₂ and 10NiO-SiO₂ samples prepared by IM or PG method were attributed to the amorphous SiO₂, which weakened and almost disappeared with increasing Cu loadings up to 80% in the CuO-SiO₂ and NiOCuO-SiO₂ samples. The apparent diffraction peaks at $2\theta = 35.6$ and $38.7°$ in the calcined 80CuO-SiO₂, 90CuO-SiO₂, 10NiO80CuO-SiO₂ and 10NiO/80CuO-SiO₂ samples indicated the presence of monoclinic phase of CuO (JCPDS 05-0661). In addition, the obvious diffraction peaks at $2\theta = 37.2$ and $43.3°$ due to NiO (JCPDS 22-1189) were

observed in 10NiO/SiO$_2$ and 10NiO/80CuO-SiO$_2$ samples prepared by IM method. Notably, no diffraction peaks assignable to NiO were observed in the XRD patterns of both 10NiO-SiO$_2$ and 10NiO80CuO-SiO$_2$ samples prepared by PG or CPG method, respectively, which could be ascribed to the high dispersion of NiO in these samples.

Fig. 3B presents the XRD profiles of the representative *in situ* reduced Cu, Ni and Ni-decorated Cu catalysts. No characteristic diffraction peaks of Ni^0 were observed in the reduced 10Ni-SiO$_2$ catalyst, while intense and strong diffraction peaks at 44.5, 51.8 and 76.4° attributable to metallic Ni^0 (JCPDS 04-0850) presented in reduced 10Ni/SiO$_2$, showing the much higher dispersion of Ni^0 in the former catalyst. As for the reduced 80Cu-SiO$_2$ and 90Cu-SiO$_2$ catalysts, the diffraction peaks of CuO disappeared, while the peaks at $2\theta = 43.3$, 50.4 and 74.1° assignable to metallic Cu^0 (JCPDS 04-0836) appeared. Different from either monometallic Ni/SiO$_2$ or Cu-SiO$_2$ catalysts, both bimetallic 10Ni80Cu-SiO$_2$ and 10Ni/80Cu-SiO$_2$ catalysts showed the diffraction peaks positioned between Ni^0 and Cu^0. Such finding indicates the formation of Cu-Ni alloy due to the successful distribution of the Ni atoms in the Cu lattice in both bimetallic catalysts, which is in agreement with the previous studies on NiCu bimetallic catalysts [51,59,60]. Moreover, both NiCu-SiO$_2$ bimetallic catalysts also gave much weaker XRD peaks compared to those in the pattern of the monometallic Cu catalysts, referring a better dispersion of Cu particles with the introduction of Ni by the formation of Cu-Ni alloys.

The mean crystalline sizes of CuO, NiO, Cu^0, Ni^0 and Cu-Ni alloy in the representative samples mentioned above were calculated by the Scherrer equation, and the results were compiled in Table 5. The CuO crystalline sizes for the calcined 80CuO-SiO$_2$, 90CuO-SiO$_2$, 10NiO80CuO-SiO$_2$ and 10NiO/80CuO-SiO$_2$ samples were in the range of 6–7 nm, with the 10NiO80CuO-SiO$_2$ sample showing the smallest size (6.0 nm). The crystalline sizes of NiO in both 10NiO-SiO$_2$ and 10NiO80CuO-SiO$_2$ samples prepared by PG method were <3 nm, while these for 10NiO/SiO$_2$ and 10NiO/80CuO-SiO$_2$ samples were 14.1 and 6.8 nm, respectively. After *in situ* reduction at 573 K for 2 h, the Cu^0 crystalline sizes for 80Cu-SiO$_2$ and 90Cu-SiO$_2$ profoundly increased to 11.1 and 11.8 nm, respectively. In contrast, the crystalline sizes of Cu-Ni alloy for 10Ni80Cu-SiO$_2$ and 10Ni/80Cu-SiO$_2$ just enlarged from 6.0 and 6.7 nm of CuO in the calcined samples to 9.3 and 10.3 nm, respectively, indicating the decoration of Ni could inhibit the sintering of Cu during the reduction treatment. Previous studies also showed that the strong interactions between Cu and Ni atoms prevent the sintering of the bimetallic catalysts [60]. According to the Vegard's law, the bulk compositions of the Cu-Ni alloy particles in terms of Ni/Cu mole ratio in 10Ni80Cu-SiO$_2$ and 10Ni/80Cu-SiO$_2$ were estimated to be 1/5.7 and 1/4.2, respectively, with the former being more close to its bulk composition (Ni/Cu = ~1/8). Such finding implies a more uniform composition of the Ni-Cu alloy nanoparticles in 10Ni80Cu-SiO$_2$ and a higher Ni surface enrichment of Ni-Cu alloy nanoparticles in 10Ni/80Cu-SiO$_2$ [52].

Fig. 4 shows the XRD patterns of the 90Cu-SiO$_2$ and 10Ni80Cu-SiO$_2$ before reaction and after 5 cycles in xylitol hydrogenolysis. Besides the apparent diffractions of Cu^0 and Cu-Ni alloy mentioned above, additional diffraction peaks at $2\theta = 14.8$, 24.3 and 30.1° attributable to CaC$_2$O$_4$·H$_2$O (JCPDS 20-0231) and the sharp diffraction peaks at $2\theta = 23.0$, 29.5 and 35.9° due to CaCO$_3$ (JCPDS 47-1743) were also observed in the used 90Cu-SiO$_2$ and 10Ni80Cu-SiO$_2$ catalysts after 5 cycles (Fig. 4A). Note that the characteristic diffraction peaks of Cu-Ni alloy were well preserved and not decomposed into separate Cu^0 and Ni^0 phases (Fig. 4B). Meanwhile, the crystallite size of Cu-Ni alloy slightly increased from 9.3 nm of the freshly reduced 10Ni80Cu-SiO$_2$ catalyst to 13.0 nm of the used catalyst after 5 runs, while that of Cu^0 for 90Cu-SiO$_2$ catalyst increased rapidly from 11.8 to 25.4 nm after the same procedure. Such findings indicate that the decoration of Ni remarkably increased the
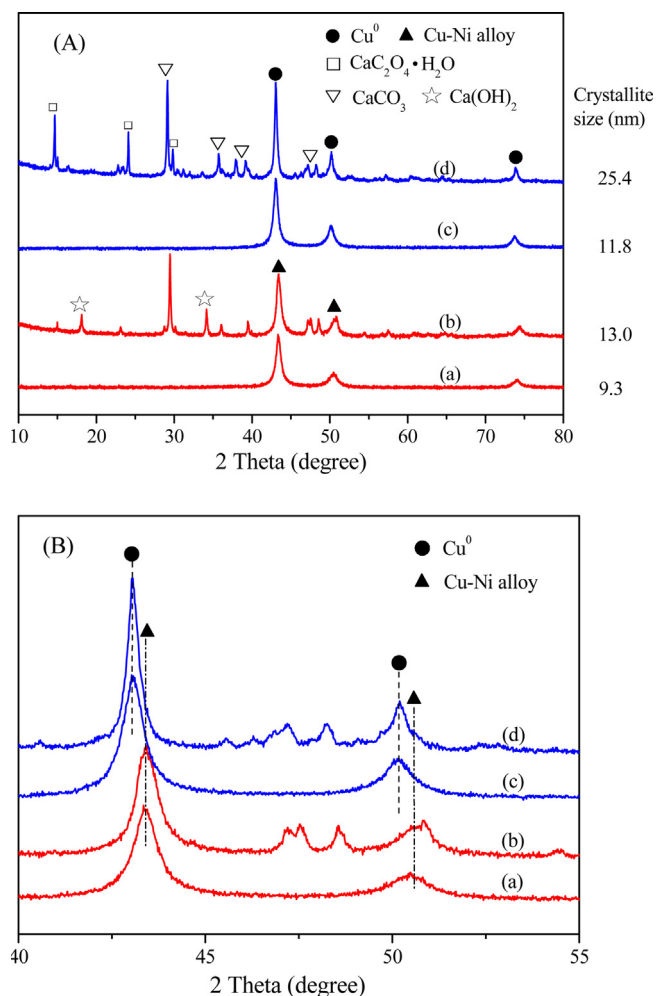

Fig. 4. XRD patterns of the (a) reduced 10Ni80Cu-SiO$_2$, (b) used 10Ni80Cu-SiO$_2$ after 5 runs, (c) reduced 90Cu-SiO$_2$, (d) used 90Cu-SiO$_2$ after 5 runs. (B) The magnified patterns.

stability of the catalyst during xylitol hydrogenolysis reaction, probably due to the formation of stable Cu-Ni alloy. In addition, the diffraction peaks of CaC$_2$O$_4$·H$_2$O in the used 10Ni80Cu-SiO$_2$ catalyst were rather weaker than those observed in the used 90Cu-SiO$_2$ catalyst, suggesting that the former catalyst could greatly inhibit the formation of CaC$_2$O$_4$·H$_2$O coke, one of the main factors for catalysts deactivation in xylitol hydrogenolysis [28].

The textural properties of the representative silica-stabilized Cu, Ni and Ni-decorated Cu samples before and after reduction in H$_2$ are given in Table 5. The actual metal loadings in these samples measured by AAS were close to the corresponding nominal loadings. The BET surface area of 10NiO80CuO-SiO$_2$ sample was 188 m^2/g, slightly higher than that of 90Cu-SiO$_2$ (167 m^2/g) and 80Cu-SiO$_2$ (176 m^2/g), probably due to that the decoration of Ni promoted the dispersion of Cu in the sample. Due to the blocking of pores by the decoration of NiO particles, the BET surface area of 10NiO/80CuO-SiO$_2$ decreased from 176 m^2/g of the mother 80CuO-SiO$_2$ to 123 m^2/g after impregnation and calcination. Similarly, the surface area for 10NiO/SiO$_2$ decreased obviously to 120 m^2/g after decoration of NiO onto SiO$_2$ support (360–410 m^2/g). The Cu dispersions (D_{Cu}) of the Cu-SiO$_2$ and Ni-decorated Cu-SiO$_2$ samples, determined by dissociative N$_2$O adsorption, decreased in the order: 10Ni80Cu-SiO$_2$ > 10Ni/80Cu-SiO$_2$ > 80Cu-SiO$_2$ > 90Cu-SiO$_2$ (Table 5), showing that the decoration of Ni could increase the dispersion of Cu, especially for the bimetallic catalyst prepared by CPG method. Previous studies also showed that the decora-

Table 5
The textural properties of representative calcined and reduced silica-stabilized Cu, Ni and Ni-decorated Cu samples.

Samples	Cu/Ni (wt%)[a]	S_{BET} (m²/g)[b]	D_{pore} (nm)[b]	Crystallite size (nm)[c]				D_{Cu} (%)[e]	S_{Cu} (m²/g)[f]	d_{Cu} (nm)[g]
				CuO	NiO	Cu⁰	Ni⁰			
10NiO-SiO₂	-/8.4	216	14.9	–	<3	–	<3	–	–	–
10NiO/SiO₂	-/8.7	120	12.4	–	14.1	–	21.7	–	–	–
80CuO-SiO₂	72.3/-	176	10.4	6.4	–	11.1	–	12.4	84.1	8.1
90CuO-SiO₂	86.6/-	167	13.9	6.8	–	11.8	–	10.0	67.8	10.0
10NiO80CuO-SiO₂	72.0/7.9	188	12.0	6.0	<3	9.3[d]		17.1	115.9	5.8
10NiO/80CuO-SiO₂	72.3/8.4	123	12.0	6.7	6.8	10.6[d]		14.3	69.8	7.0

[a] Determined by AAS.
[b] BET method.
[c] Calculated from the Scherrer equation. The crystallite sizes of CuO and NiO were for calcined samples, while those of Cu⁰ and Ni⁰ were for reduced active catalysts.
[d] For Cu-Ni alloy.
[e] Cu dispersion obtained from dissociative N₂O adsorption.
[f] Cu surface area obtained from dissociative N₂O adsorption.
[g] Mean Cu particle size calculated from dissociative N₂O adsorption.

tion of oxidative nickel species was helpful for improving the dispersion of copper in Ni-Cu bimetallic samples [46]. Based on Cu dispersion, the Cu surface areas (S_{Cu}) of the Cu-SiO₂ and Ni-decorated Cu-SiO₂ catalysts varied in the range of 69.8–115.9 m²/g, with that of the 10Ni80Cu-SiO₂ catalyst presented the highest value. Additionally, the Cu particle sizes (d_{Cu}) of the Cu-SiO₂ and Ni-decorated Cu-SiO₂ samples increased in the order 10Ni80Cu-SiO₂ < 10Ni/80Cu-SiO₂ < 80Cu-SiO₂ < 90Cu-SiO₂ (Table 5) from 5.8 to 10.0 nm, which is in line with the above XRD results.

Fig. 5 shows the representative TEM images of reduced 80Cu-SiO₂, 90Cu-SiO₂, 10Ni80Cu-SiO₂ and 10Ni/80Cu-SiO₂ catalysts. Dispersed Cu nanoparticles with sizes around 3–10 nm together with some nanoparticles composed of short nanorods were observed in both 80Cu-SiO₂ and 90Cu-SiO₂ catalysts. Noticeably, the decoration of Ni by CPG method resulted in a more even dispersion of metal nanoparticles, and the nanoparticles composed of short nanorods largely disappeared (Fig. 5C). The short nanorods were also largely restrained by the decoration of Ni by IM method (Fig. 5D). The average particle sizes in 80Cu-SiO₂, 90Cu-SiO₂, 10Ni80Cu-SiO₂ and 10Ni/80Cu-SiO₂ catalysts were 9.8, 10.3, 7.8 and 8.2 nm, respectively, which show similar tendency with XRD and N₂O chemisorption results (Table 5). Such findings revealed that the decoration of Ni could further decrease the particle size and thus increase the dispersion of Cu, especially for the catalyst prepared by CPG method. Further investigation of the HRTEM images of single particles from reduced 10Ni80Cu-SiO₂ and 10Ni/80Cu-SiO₂ catalysts (Fig. 5E and F) showed lattice fringes of about 0.2062–0.2070 nm, which located just right between 0.2034 nm for metallic Ni(111) and 0.2088 nm for metallic Cu(111), indicating the formation of face-centred cubic (fcc) Cu-Ni alloy in both catalysts [47,48]. The elemental EDS maps shown in Figure S1 also support the formation of Cu-Ni alloys in both bimetallic catalysts. The composition of Cu-Ni alloys in terms of Ni/Cu mole ratio estimated from the lattice distances of 10Ni80Cu-SiO₂ and 10Ni/80Cu-SiO₂ catalysts were 1/2.0 and 1/1.1, respectively, which were 3 and 4 times that of the corresponding Ni/Cu mole ratio calculated from the XRD results based on the Vegard's law. Such an obvious discrimination between HRTEM and XRD results further supported the surface enrichment of Ni in the Cu-Ni alloy particles especially in 10Ni/80Cu-SiO₂ catalyst prepared by IM method.

The surface chemical states and compositions of the calcined and *in situ* reduced silica-stabilized monometallic Cu, Ni and bimetallic Ni-Cu samples were characterized by XPS spectra. Fig. 6A shows the Cu2p spectra of different calcined Cu-containing samples. The intense and broad photoelectron peaks in the range of 933.8–934.7 eV along with the presence of the characteristic shakeup satellite peaks in the range of 940–945 eV suggest that the copper species in all samples existed in +2 valence state. Accord-

ing to our previous findings, the positive binding energy (B.E.) shift of the Cu2p3/2 core level for 80CuO-SiO₂ and 90CuO-SiO₂ samples prepared by PG method, relative to B.E. of pure CuO at 933.4 eV, demonstrates the formation of copper phyllosilicate with strong metal-support interaction (SMSI) [28,61]. The Cu2p3/2 peak of 10NiO80CuO-SiO₂ sample shifted obviously from 933.8 eV for 80CuO-SiO₂ and 90CuO-SiO₂ to a higher level of ~934.7 eV, and a shoulder peak at ~934.7 eV was also observed in the Cu2p3/2 spectra of 10NiO/80CuO-SiO₂. Such noticeable positive B.E. shift of the Cu2p core level for the NiO-decorated 80CuO-SiO₂ samples prepared by both IM and CPG methods might be ascribed to the increase in interaction of copper species with not only silica but also nickel [46]. Therefore, based on XRD (Fig. 3A) and XPS characterizations there were CuO and amorphous copper phyllosilicate present in the calcined 80CuO-SiO₂ and 90CuO-SiO₂ samples; while for the Ni-decorated 80CuO-SiO₂, there were additional present the copper interacted nickel species, besides CuO and copper phyllosilicate.

Similarly, for all calcined Ni-containing samples (Fig. 6B), the presence of Ni2p3/2 core levels in the range 854.4–856.3 eV and the intense satellite peaks above the primary photo lines indicate the presence of divalent nickel compounds [46]. For 10NiO/SiO₂ sample, its Ni2p3/2 B.E. (854.4 eV) is very close to the value of pure NiO (~854.5 eV), inferring the presence of NiO interacted weakly with SiO₂ [63]. Except for this peak, an additional shoulder peak at higher B.E. region (~856.0 eV) was also observed in the 10NiO/80CuO-SiO₂, which might be attributed to Ni²⁺ ions surrounded by Cu²⁺ (through O²⁻ linkage) [46]. A relatively large shift of the Ni2p3/2 B.E. of calcined 10NiO-SiO₂ sample prepared by PG method to ~856.3 eV was seen, referring to nickel specie with much stronger metal-support interaction [62]. The high Ni2p3/2 B.E. of calcined 10NiO80CuO-SiO₂ might be contributed by the presence of Ni²⁺ interacted strongly with both the silica and Cu²⁺ surrounded. In addition, the surface Ni/Cu atom ratios determined by XPS were 1/3.6 and 1/2.2 for calcined 10NiO80CuO-SiO₂ and 10NiO/80CuO-SiO₂ samples, respectively. These values are much higher than these of the bulk Ni/Cu ratios (~1/8.0) determined by AAS (Table 5), indicating a pronounced surface enrichment of Ni on these two samples [46], especially for the 10NiO/80CuO-SiO₂ prepared by IM method. This result also reveals that the Ni species were dispersed more evenly in 10NiO80CuO-SiO₂ in comparison with 10NiO/80CuO-SiO₂. Clearly, these findings are in agreement with the above XRD and TEM characterizations.

After reduction *in situ* at 573 K in H₂ atmosphere for 2 h, the satellite peaks for Cu2p and Ni2p in all calcined samples disappeared (Fig. 6C and D), and the B.E.s of Cu2p3/2 and Ni2p3/2 core levels decreased to the range of 932.1–932.5 eV and 852.3–853.0 eV, respectively. Such findings together with the *in situ*
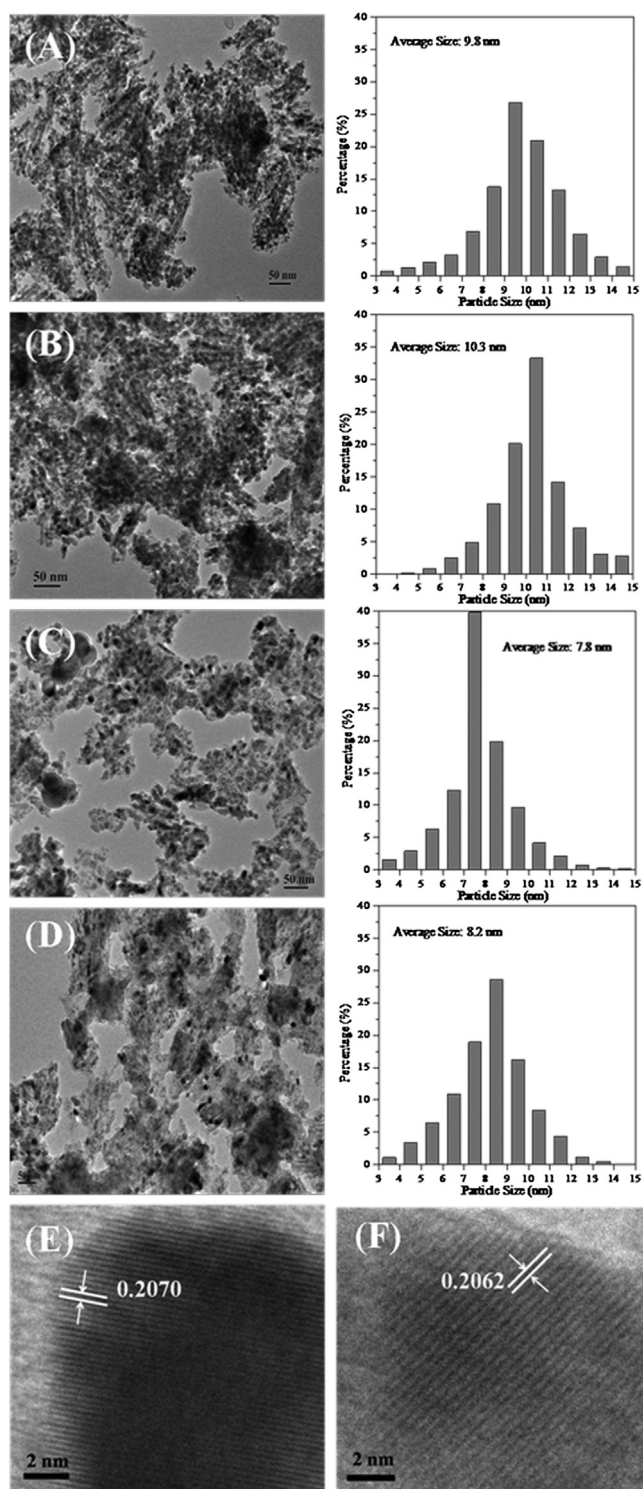
Fig. 5. TEM images and particle size distribution of reduced (A) 80Cu-SiO$_2$, (B) 90Cu-SiO$_2$, (C) 10Ni80Cu-SiO$_2$ and (D) 10Ni/80Cu-SiO$_2$ catalysts. HRTEM images of (E) 10Ni80Cu-SiO$_2$ and (F) 10Ni/80Cu-SiO$_2$.

XRD results (Fig. 3B) indicate that the Cu^{2+} and Ni^{2+} in all samples were reduced predominantly to metallic state [46]. The differences in B.E.s of both Cu2p3/2 and Ni2p3/2 core levels might be aroused from the different electronic interactions between copper and nickel species. For reduced monometallic Cu-SiO$_2$ catalysts, the B.E.s of Cu are 932.1 eV, while for bimetallic NiCu catalysts, the B.E.s of Cu are 932.5 eV; for reduced monometallic Ni catalysts, the B.E.s of Ni are 853.0 eV, while for bimetallic Ni-Cu, the B.E.s of

Ni are 852.3 eV. The increase in B.E. of Cu with the simultaneous decrease in B.E. of Ni for bimetallic NiCu-SiO$_2$ in comparison with the monometallic catalysts might be related to the charge transfer from Cu to the adjacent Ni [46,63]. This finding also points out the formation of Cu-Ni alloy in the bimetallic catalysts.

Fig. 7 shows the TPR patterns of the representative calcined silica-stabilized CuO, NiO and NiOCuO bimetallic samples. The 10NiO-SiO$_2$ prepared by PG method presented a main reduction peak centered at ∼603 K, while the 10NiO/SiO$_2$ sample showed two overlapping reduction peaks centered at higher temperatures of about 619 and 645 K. Based on the XRD (Fig. 3A and Table 5) and XPS results (Fig. 6B), it is reasonable that the main H$_2$ consumption peak for 10NiO-SiO$_2$ is ascribed to the reduction of highly dispersed Ni^{2+} species, while the two reduction peaks for 10NiO/SiO$_2$ are attributed to the reduction of dispersed NiO with smaller size and bulk NiO with larger size, respectively.

The 80CuO-SiO$_2$ and 90CuO-SiO$_2$ samples showed a similar asymmetric main reduction peak at around 530 K. According to literature [64] and our previous findings [61,65], this peak could be ascribed to the collective contribution of stepwise reduction of dispersed CuO to Cu^0 and the partially reduction of copper species with SMSI to Cu$^+$. It is interesting to find that the main reduction peak for both 10NiO80CuO-SiO$_2$ and 10NiO/80CuO-SiO$_2$ shifted 5–15 K to lower temperature region versus monometallic CuO-SiO$_2$ samples, with the shift of the former sample more obvious. Additionally, no other H$_2$ consumption could be observed at temperatures above 580 K for both bimetallic samples, even though they decorated the similar amount of Ni as 10NiO-SiO$_2$ and 10NiO/SiO$_2$ samples. Such findings reveal that the reduction of both nickel and copper species was remarkably enhanced in the Ni-Cu bimetallic samples and that the Cu-Ni alloy could be generated even at much lower reduction temperatures [63], which was also supported by the in situ XRD (Fig. 3B) and XPS (Fig. 6C and D) reduction results. Moreover, the 10NiO80CuO-SiO$_2$ also presented a relatively narrower H$_2$ consumption region in comparison with 10NiO/80CuO-SiO$_2$, inferring that the two metallic species in the former sample were more homogeneously dispersed.

4. Discussion

4.1. The effect of Ni decoration on the structure and surface properties of Cu-SiO$_2$ catalysts

Clearly, the above characterizations showed that the decoration of Ni profoundly affected the structure and surface properties of Cu-SiO$_2$ catalysts. One of the most noticeable features of the Ni-decorated Cu-SiO$_2$ catalysts is the increased Cu dispersion and thus decreased the domains of the active particles, especially for the NiCu-SiO$_2$ bimetallic catalyst prepared by CPG method, as can be verified from XRD (Fig. 3), textural (Table 5) and TEM (Fig. 5) characterizations. As a result, the decoration of Ni promoted the interaction between not only Cu and silica, but also Cu and Ni species (facilitated the formation of copper interacted nickel species, Fig. 6A), favoring the generation of a larger amount of active sites with smaller ensemble sizes after reduction treatment and maintaining the stability of the bimetallic catalysts in xylitol hydrogenolysis.

Another important feature of Ni-decoration is the enhancement in the reducibility of the bimetallic samples as evidenced from H$_2$-TPR results shown in Fig. 7. It is known that Cu^{2+} has a higher standard reduction potential than that of Ni^{2+} (+0.34 eV for Cu^{2+} → Cu vs. −0.25 eV for Ni^{2+} → Ni^0) [44,47,66]. Thus, Cu^{2+} is more easily reduced than Ni^{2+} at similar conditions (as exactly observed in our cases, Fig. 7), and subsequently, the reduced Cu can act as a catalyst to promote the reduction of Ni^{2+}. In the meantime,
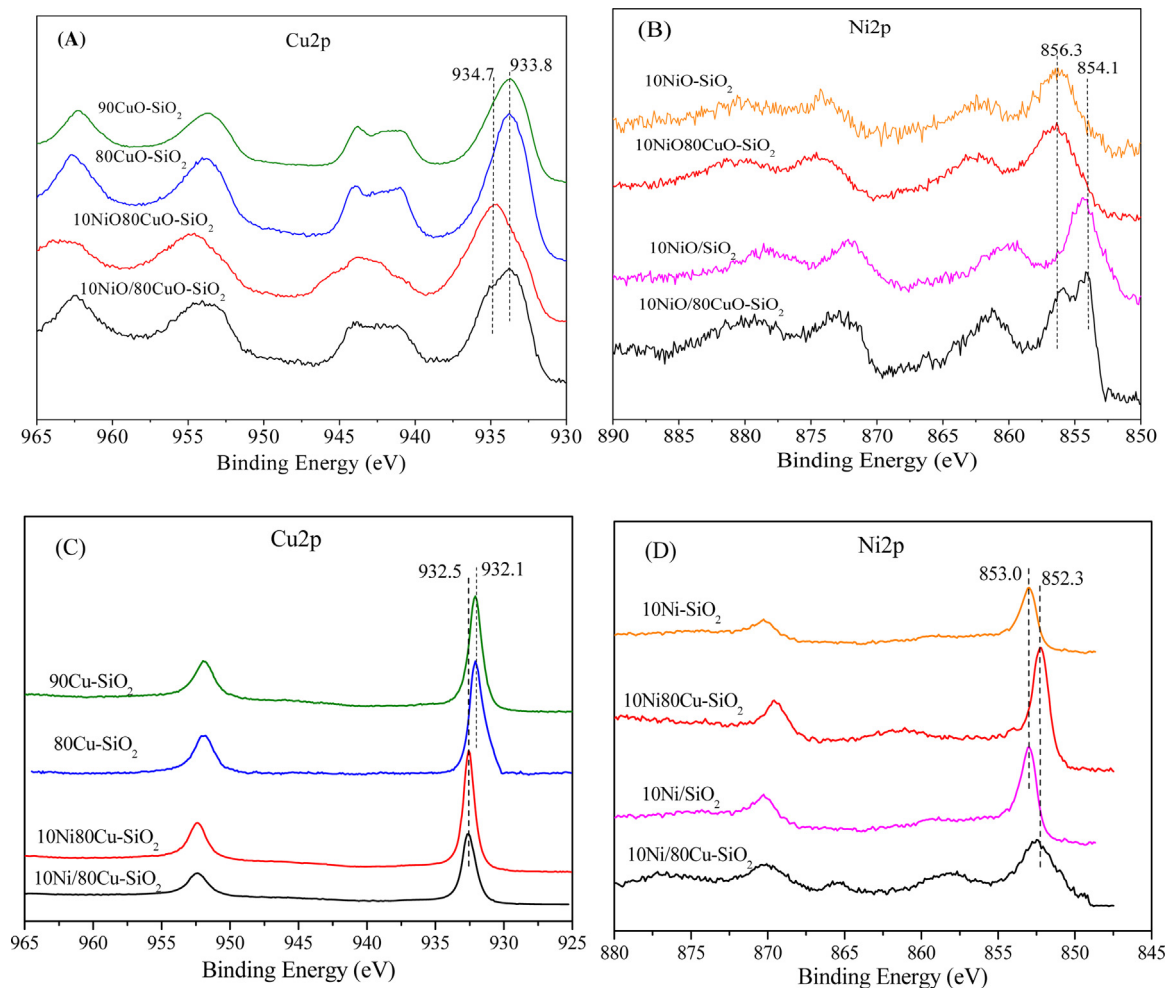
Fig. 6. XPS patterns of Cu2p (A: calcined; C: *in situ* reduced) and Ni2p (B: calcined; D: *in situ* reduced) for different samples.

the reduced Ni species could be considered as a co-active site that can accelerate the adsorption and activation of H_2, thus helping the shift of reduction temperature to lower temperature regions for the bimetallic samples. The increase in reducibility of the Ni-decorated 80Cu-SiO$_2$ catalysts suggests these catalysts have lower barrier for H_2 activation, which facilitates the dissociation of H_2 and increases the concentration of active hydrogen accessing the carbonyl reaction intermediates during xylitol hydrogenolysis. Additionally, the enhancement in reducibility of the NiCu-SiO$_2$ bimetallic catalysts may favors the generation of a larger amount of active metal/alloy sites for hydro–dehydrogenation reactions. Obviously, such property would greatly enhance the hydro-dehydrogenation ability of the bimetallic catalysts and have a noticeable beneficial influence on the overall hydrogenolysis reaction.

Moreover, the decoration of Ni also resulted in the formation of Ni surface-enriched Cu-Ni alloy particles in both 10Ni80Cu-SiO$_2$ and10Ni/80Cu-SiO$_2$ catalysts, as inferred from XRD (Fig. 3), HRTEM (Fig. 5E and F) and XPS (Fig. 6) characterizations. The formation of such "core-shell" like alloy nanoparticles in the reduced bimetallic catalysts is probably due to the different redox potentials of Cu^{2+} and Ni^{2+} as mentioned above, which resulted in the first formation of Cu-rich core at low reduction temperature, followed by the Ni-rich Cu-Ni alloy shell on the surface of the Cu-rich core with increasing reducing temperature [67,68]. Despite a surface enrichment with copper whose energy is lower (1.84 J/m^2 at 0 K) than that of nickel (2.01 J/m^2 at 0 K) is often reported for Ni-Cu alloy particles [52,69–71], Ni surface-enriched Cu-Ni alloy in

our cases could be produced due to different preparation methods and pretreatment conditions [46,47,51,72]. The formation of nickel surface enriched Cu-Ni alloy might greatly improve the dispersion of the copper species and tremendously enhance the catalytic hydrogenolysis performance of the CuNi-SiO$_2$ bimetallic catalysts, as reported previously [46,47,51]. What's more, the formation of Cu-Ni alloy would provide active sites that outperform the activity of their monometallic counterparts due to the electronic effects between metals, which could alter the bonding properties of the Cu-Ni alloy surfaces. The electron transfer from Ni to Cu in the NiCu-SiO$_2$ bimetallic catalysts (determined by XPS characterization, Fig. 6D), analogizing the electron transfer from Pd to Cu in a PdCu/ZrO$_2$ bimetallic catalyst for sorbitol hydrogenolysis [23], would profoundly promote the activity and target glycol selectivity in xylitol hydrogenolysis.

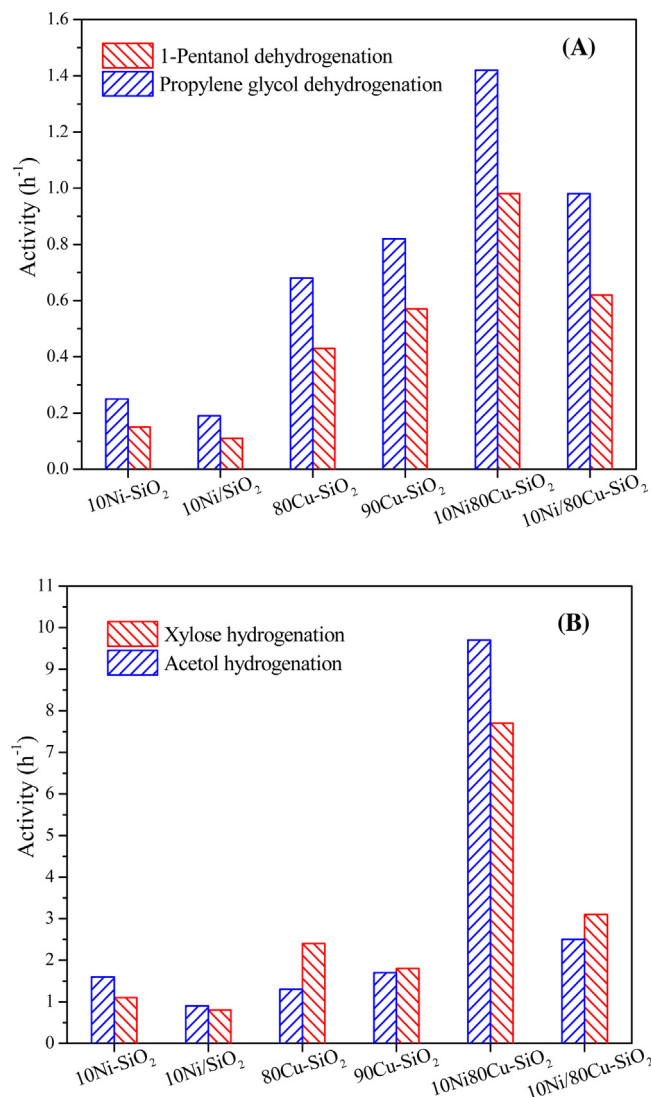### 4.2. The effect of Ni decoration on the catalytic properties of Cu-SiO$_2$ catalysts

As can be clearly seen from Tables 2–3, most of the Ni-decorated Cu-SiO$_2$ bimetallic catalysts were more active and selective than monometallic Ni-SiO$_2$ and Cu-SiO$_2$ catalysts in the hydrogenolysis of xylitol to ethylene glycol and propylene glycol. Such an enhancement in catalytic activity and selectivity would be associated with their C–OH dehydrogenation and C=O hydrogenation activities, due to the reaction rate of C$_5$ and C$_6$ polyols hydrogenolysis is governed by the C–OH dehydrogena-
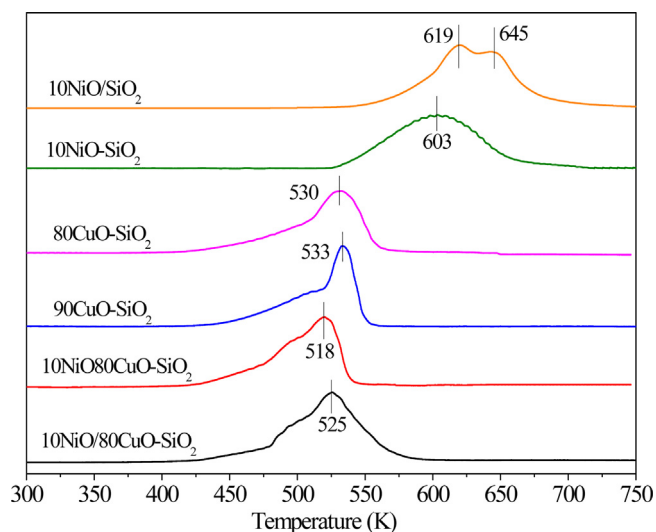
Fig. 7. H_2-TPR profiles of the representative calcined silica-stabilized CuO, NiO and NiOCuO bimetallic samples.

Fig. 8. The dehydrogenation activity for 1-pentanol and propylene glycol (A) and the hydrogenation activity for xylose and acetol over Cu-SiO$_2$, Ni-SiO$_2$ and Ni-decorated Cu-SiO$_2$ catalysts (B). Reaction conditions: 473 K, 3 MPa N$_2$, 0.072–0.108 g metals, ~5% conversion (dehydrogenation reactions); 353 K, 6 MPa H$_2$, 0.036–0.144 g metals, 40 g 10 wt% substrate aqueous solution, ~30% conversion (hydrogenation reactions). Activity is defined as the mol of converted substrate per mol of metals loaded in the catalyst per time.

tion step [7,18], while the glycol selectivities are depended on the hydrogenation of the carbonyl intermediates [7,9]. Notably, the decoration of Ni greatly promoted both the C–OH dehydrogenation and C=O hydrogenation activities of the NiCu-SiO$_2$ bimetallic catalysts, based on the probe reactions of C–OH dehydrogenation and C=O hydrogenation shown in Fig. 8. Both the dehydrogenation activities (Fig. 8A) and the hydrogenation activities (Fig. 8B) of the catalysts increased in the order of 10Ni-SiO$_2$ ≈ 10Ni/SiO$_2$ < 80Cu-SiO$_2$ < 90Cu-SiO$_2$ < 10Ni/80Cu-SiO$_2$ < 10Ni80Cu-SiO$_2$, revealing the much higher hydro-dehydrogenation activity of Ni-Cu bimetallic catalysts. The dehydrogenation activities achieved on 10Ni80Cu-SiO$_2$ catalyst were around 2 times higher than those obtained on 80Cu-SiO$_2$, while the hydrogenation activities on the former were 3.2 or 7.5 time that of the latter showing that Ni-decoration could more profoundly promote the hydrogenation activity of the Cu catalyst as compared with its dehydrogenation activities. Therefore, the simultaneous increase in both C–OH dehydrogenation and C=O hydrogenation activities, especially noticeable in hydrogenation activity of the NiCu-SiO$_2$ bimetallic catalysts due to the promotion effect of Ni on the structure and surface properties of Cu-SiO$_2$ mentioned above ultimately promoted the overall xylitol hydrogenolysis activity and target glycols selectivity, as can be clearly seen from Table 3.

Many studies ascribed the increased catalytic performance of the NiCu bimetallic catalysts to the synergetic effect between Cu and Ni [48,50,73]. In our case, characterization of the NiCu-SiO$_2$ bimetallic catalysts showed the formation of Cu-Ni alloy in both 10Ni80Cu-SiO$_2$ and 10Ni/80Cu-SiO$_2$ catalysts after reduction in H$_2$. In addition, such alloy structure was well preserved after xylitol hydrogenolysis reaction under high pressure and hydrothermal conditions (Fig. 3). Therefore, it is reasonable that the formation of highly dispersed Ni surface-enriched Cu-Ni alloy sites, which presented much higher hydro-dehydrogenation reactivity relative to monometallic Cu^0 or Ni^0 sites, enhanced the activity and selectivity of the Ni-Cu bimetallic catalysts in xylitol hydrogenolysis. Previous studies [47,52,74] also demonstrated that the formation of Cu-Ni alloy sites plays key roles in improving the catalytic performances. Taking the above analysis into consideration, the highest activity and glycols selectivity of 10Ni80Cu-SiO$_2$ catalyst would be ascribed to its high metal dispersion and the alloy formation whose surface Cu/Ni ratio might result in good balance of C–OH dehydrogenation activity and C=O bond hydrogenation activity.

Furthermore, a remarkable increase in the stability of the Ni-decorated 80Cu-SiO$_2$ catalyst was observed in comparison with 90Cu-SiO$_2$ catalyst (Fig. 2). The formation of Cu-Ni alloy is reported to promote the thermal stability and reaction stability of the catalyst [49,75]. Therefore, the profound enhancement in recyclability for the 10Ni80Cu-SiO$_2$ can be ascribed tentatively to its increased metal dispersion and highly dispersed and stable Cu-Ni alloy (Fig. 4), which consequently retarded the sintering of the active metal sites. The significant increase in hydrogenation activity of the 10Ni80Cu-SiO$_2$ bimetallic catalyst (Fig. 8B), which promoted the hydrogenation of the carbonyl intermediates from base-catalyzed retro-aldol condensation to the desired target glycols, would largely decrease the formation of acid byproducts and cokes (Fig. 4A), and thus to some extent contributes to the good reusability of the bimetallic catalyst.
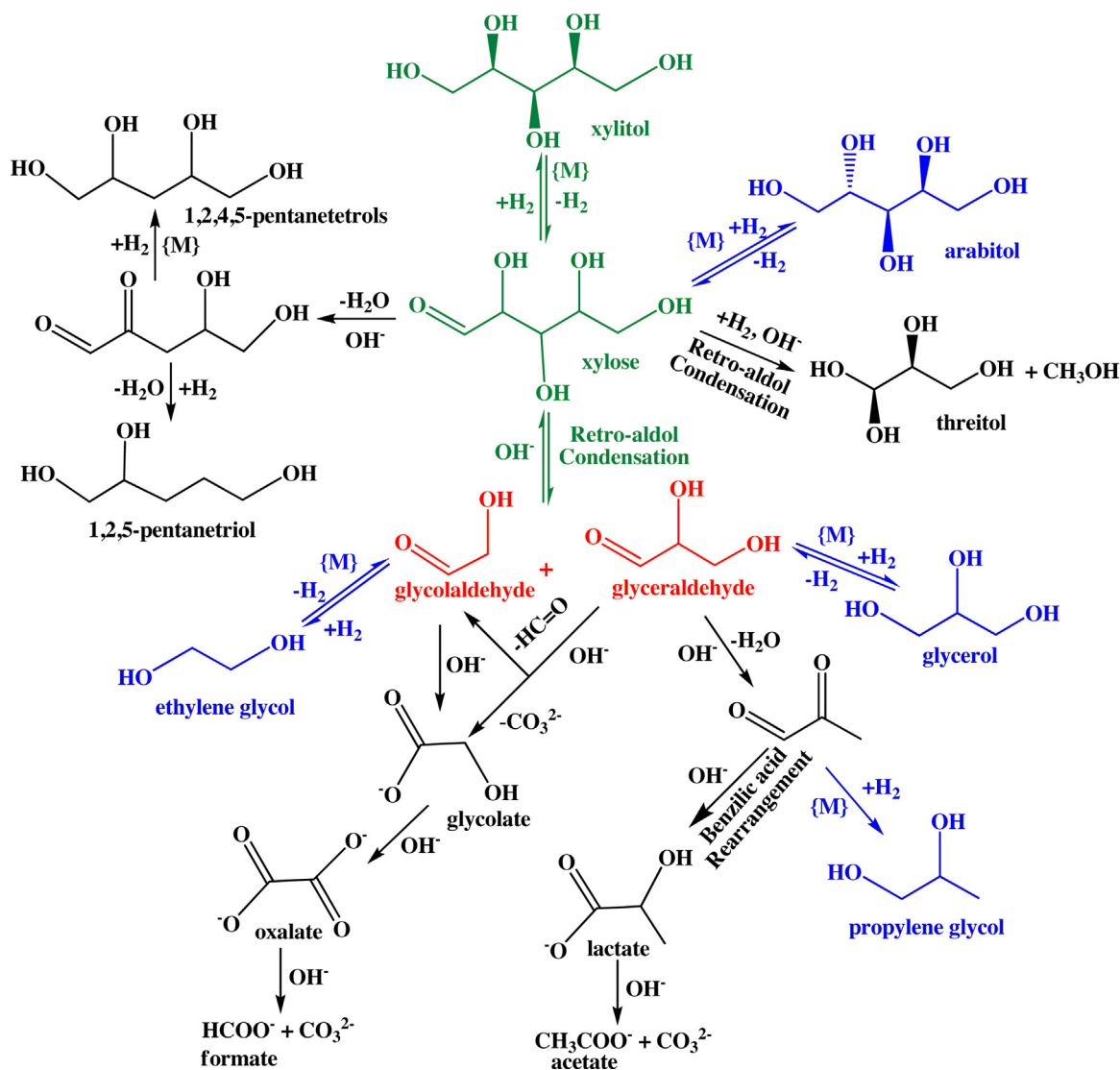
Scheme 2. Proposed reaction pathways of xylitol hydrogenolysis over CuNi-SiO$_2$ catalyst under basic conditions.

4.3. The reaction pathways of xylitol hydrogenolysis over CuNi-SiO$_2$ bimetallic catalyst

Based on the products distribution and the effect of reaction parameters on catalytic conversions and product selectivities (Table 4 and Fig. 1) and also our previous studies [9,28] on catalytic hydrogenolysis of xylitol on monometallic Cu-SiO$_2$ catalysts, we proposed the reaction pathways of xylitol hydrogenolysis over CuNi-SiO$_2$ catalyst under basic conditions in Scheme 2. Similar to the reaction pathways previously proposed for xylitol hydrogenolysis over Ru/C by Sun and Liu [7], the main reaction involves the dehydrogenation of xylitol to xylose on metal/bimetal sites as the rate-determining step, followed by the retro-aldol condensation of xylose with Ca(OH)$_2$ to the key reaction intermediates of glycolaldehyde and glyceraldehyde, and their subsequent hydrogenation to ultimately form glycols. In the presence of Ca(OH)$_2$, glycolaldehyde and glyceraldehyde can be separately transformed to the acid byproducts of glycolic acid and lactic acid, which are in competition with the hydrogenation reaction to the target two glycols. Glycolic acid and lactic acid can be further converted to CaC$_2$O$_4$, formic acid, acetic acid and CaCO$_3$ under a high-basicity hydrothermal condition [28,76]. Arabitol, an isomer of xylitol formed via hydrogenation of the xylose intermediate, can be more facilely

converted to the target glycols and other byproducts than xylitol [23]. Glycerol, a hydrogenation product of glyceraldehyde, can be transformed back to glyceraldehyde and further to other C$_2$ and C$_3$ glycols and acid byproducts. The other main byproducts detected are dehydrated pentitols, including 1,2,5-pentanetriols and 1,2,4,5-pentanetetrols. They were formed by the dehydration and hydrogenation of xylose, probably through a dehydration of α,β-hydroxylcarbonyl mechanism [39]. Such complex reaction networks along with the high reactivity of the carbonyl intermediates make it very difficult to achieve high glycols yield in xylitol hydrogenolysis, which also show the importance in developing of highly active hydro-dehydrogenation catalysts.

5. Conclusion

Ni-decorated Cu-SiO$_2$ bimetallic catalysts presented notably superior activity, selectivity and stability to their counterparts of monometallic Cu-SiO$_2$ and Ni-SiO$_2$ catalysts in the hydrogenolysis of biomass-derived xylitol to ethylene glycol and propylene glycol in the presence of Ca(OH)$_2$. The catalytic activity and selectivity of the NiCu bimetallic catalysts depended largely on its Cu/Ni ratios and the Ni decoration methods (impregnation or co-precipitation). A high combined ethylene glycol and propylene glycol selectivity

of ~81% was achieved at ~100% xylitol conversion on 10Ni80Cu-SiO$_2$ prepared by co-precipitation-gel method at 473 K and 8 MPa H$_2$. The decoration of proper amount of Ni into Cu-SiO$_2$ catalysts greatly enhanced the dispersion of Cu and the reducibility of the bimetallic catalysts, and also led to the formation of highly active Cu-Ni alloy sites, relative to monometallic Cu or Ni catalysts. These bimetallic catalysts presented much higher C–OH dehydrogenation and C=O hydrogenation activities to enhance their overall performances (including activity, glycol selectivity and stability) in xylitol hydrogenolysis. These findings will shed light on the development of more efficient and stable bimetallic nanocatalysts particularly for hydrogenation and hydrogenolysis transformations of biomass-derived platform compounds.

Acknowledgement

Appendix A. Supplementary data

Supplementary data associated with this article can be found, in the online version, at http://dx.doi.org/10.1016/j.apcatb.2017.08.022.

References

[1] G.W. Huber, S. Iborra, A. Corma, Chem. Rev. 106 (2006) 4044–4098.
[2] D.M. Alonso, S.G. Wettstein, J.A. Dumesic, Chem. Soc. Rev. 41 (2012) 8075–8098.
[3] A.M. Ruppert, K. Weinberg, R. Palkovits, Angew. Chem. Int. Ed. 51 (2012) 2564–2601.
[4] M. Besson, P. Gallezot, C. Pinel, Chem. Rev. 114 (2014) 1827–1870.
[5] C. Li, X. Zhao, A. Wang, G.W. Huber, T. Zhang, Chem. Rev. 115 (2015) 11559–11624.
[6] I.T. Clark, Ind. Eng. Chem. 50 (1958) 1125–1126.
[7] J. Sun, H. Liu, Green Chem. 13 (2011) 135–142.
[8] L. Ye, X. Duan, H. Lin, Y. Yuan, Catal. Today 183 (2012) 65–71.
[9] Z. Huang, J. Chen, Y. Jia, H. Liu, C. Xia, H. Liu, Appl. Catal. B: Environ. 147 (2014) 377–386.
[10] G.W. Huber, R.D. Cortright, J.A. Dumesic, Angew. Chem. Int. Ed. 43 (2004) 1549–1551.
[11] S. Liu, Y. Okuyama, M. Tamura, Y. Nakagawa, A. Imai, K. Tomishige, Catal. Today 269 (2016) 122–131.
[12] Q. Zhang, J. Tan, T. Wang, Q. Zhang, L. Ma, S. Qiu, Y. Weng, Fuel 165 (2016) 152–158.
[13] A. Yamaguchi, N. Hiyoshi, O. Sato, M. Shirai, Green Chem. 13 (2011) 873–881.
[14] C. Pavlik, A. Onorato, S. Castro, M. Morton, M. Peczuh, M.B. Smith, Org. Lett. 11 (2009) 3722–3725.
[15] https://www.grandviewresearch.com/press-release/global-ethylene-glycols-market.
[16] https://mcgroup.co.uk/news/20140418/propylene-glycol-market-reach-supplydemand-balance-2015.html.
[17] X. Guo, J. Guan, B. Li, X. Wang, X. Mu, H. Liu, Sci. Rep. 5 (2015) 16451–16459.
[18] K.L. Deutsch, D.G. Lahr, B.H. Shanks, Green Chem. 14 (2012) 1635–1642.
[19] I. Murillo Leo, M. López Granados, J.L.G. Fierro, R. Mariscal, Appl. Catal. B: Environ. 185 (2016) 141–149.
[20] P.J.C. Hausoul, L. Negahdar, K. Schute, R. Palkovits, ChemSusChem 8 (2015) 3323–3330.
[21] L. Zhao, J. Zhou, Z. Sui, X. Zhou, Chem. Eng. Sci. 65 (2010) 30–35.
[22] M. Rivière, N. Perret, A. Cabiac, D. Delcroix, C. Pinel, M. Besson, ChemCatChem 9 (2017) 2145–2159.
[23]. Y. Jia, H. Liu, Chin. J. Catal. 36 (2015) 1552–1559.
[24] M. Banu, S. Sivasanker, T.M. Sankaranarayanan, P. Venuvanalingam, Catal. Commun. 12 (2011) 673–677.
[25] X. Chen, X. Wang, S. Yao, X. Mu, Catal. Commun. 39 (2013) 86–89.
[26] J. Sun, H. Liu, Catal. Today 234 (2014) 75–82.
[27] J. Zhang, F. Lu, W. Yu, J. Chen, S. Chen, J. Gao, J. Xu, Catal. Today 234 (2014) 107–112.
[28] H. Liu, Z. Huang, C. Xia, Y. Jia, J. Chen, H. Liu, ChemCatChem 6 (2014) 2918–2928.
[29] X. Jin, J. Shen, W. Yan, M. Zhao, P.S. Thapa, B. Subramaniam, R.V. Chaudhari, ACS Catal. 5 (2015) 6545–6558.
[30] B. Blanc, A. Bourrel, P. Gallezot, T. Haas, P. Taylor, Green Chem. 2 (2000) 89–91.
[31] Z. Wu, Y. Mao, X. Wang, M. Zhang, Green Chem. 13 (2011) 1311–1316.
[32] M.A. Dasari, P.P. Kiatsimkul, W.R. Sutterlin, G.J. Suppes, Appl. Catal. A: Gen. 281 (2005) 225–231.
[33] Z. Huang, F. Cui, H. Kang, J. Chen, X. Zhang, C. Xia, Chem. Mater. 20 (2008) 5090–5099.
[34] S. Xia, R. Nie, X. Lu, L. Wang, P. Chen, Z. Hou, J. Catal. 296 (2012) 1–11.
[35] N.D. Kim, J.R. Park, D.S. Park, B.K. Kwak, J. Yi, Green Chem. 14 (2012) 2638–2646.
[36] Z. Huang, H. Liu, Y. Jia, C. Xia, J. Chen, H. Liu, J. Mol. Catal. (China) 29 (2015) 207–217.
[37] Y. Jia, H. Liu, Catal. Sci. Technol. 6 (2016) 7042–7052.
[38] T. Soták, T. Schmidt, M. Hronec, Appl. Catal. A: Gen. 459 (2013) 26–33.
[39] K. Wang, M.C. Hawley, T.D. Furney, Ind. Eng. Chem. Res. 34 (1995) 3766–3770.
[40] L. Zhao, J.H. Zhou, H. Chen, M.G. Zhang, Z.J. Sui, X.G. Zhou, Korean J. Chem. Eng. 27 (2010) 1412–1418.
[41] M. Sankar, N. Dimitratos, P.J. Miedziak, P.P. Wells, C.J. Kiely, G.J. Hutchings, Chem. Soc. Rev. 41 (2012) 8099–8139.
[42] S. De, J. Zhang, R. Luque, N. Yan, Energy Environ. Sci. 9 (2016) 3314–3347.
[43] F. Studt, F. Abild-Pedersen, Q. Wu, A.D. Jensen, B. Temel, J.D. Grunwaldt, J.K. Nørskov, J. Catal. 293 (2012) 51–60.
[44] Q. Wu, W.L. Eriksen, L.D.L. Duchstein, J.M. Christensen, C.D. Damsgaard, J.B. Wagner, B. Temel, J.D. Grunwaldt, A.D. Jensen, Catal. Sci. Technol. 4 (2014) 378–386.
[45] K. Xiao, X. Qi, Z. Bao, X. Wang, L. Zhong, K. Fang, M. Lin, Y. Sun, Catal. Sci. Technol. 3 (2013) 1591–1602.
[46] A. Yin, C. Wen, X. Guo, W.-L. Dai, K. Fan, J. Catal. 280 (2011) 77–88.
[47] J. Wu, G. Gao, J. Li, P. Sun, X. Long, F. Li, Appl. Catal. B: Environ. 203 (2017) 227–236.
[48] B. Cai, X.-C. Zhou, Y.-C. Miao, J.-Y. Luo, H. Pan, Y.-B. Huang, ACS Sustain. Chem. Eng. 5 (2017) 1322–1331.
[49] J. Shan, N. Janvelyan, H. Li, J. Liu, T.M. Egle, J. Ye, M.M. Biener, J. Biener, C.M. Friend, M. Flytzani-Stephanopoulos, Appl. Catal. B: Environ. 205 (2017) 541–550.
[50] S.P. Patil, J.V. Pande, R.B. Biniwale, Int. J. Hydrogen Energy 38 (2013) 15233–15241.
[51] L.-C. Chen, S.D. Lin, Appl. Catal. B: Environ. 106 (2011) 639–649.
[52] D. Li, M. Lu, K. Aragaki, M. Koike, Y. Nakagawa, K. Tomishige, Appl. Catal. B: Environ. 192 (2016) 171–181.
[53] J. Greeley, M. Mavrikakis, J. Phys. Chem. B 109 (2005) 3460–3471.
[54] E.A. Cepeda, U. Iriarte-Velasco, B. Calvo, I. Sierra, J. Am. Oil Chem. Soc. 93 (2016) 731–741.
[55] A.F. Trasarti, N.M. Bertero, C.R. Apesteguía, A.J. Marchi, Appl. Catal. A: Gen. 475 (2014) 282–291.
[56] R. Jenkins, R.L. Snyder, Introduction to X-ray Powder Diffractometry, John Wiley & Sons, New York, 1996.
[57] C.J.G. Van Der Grift, A.F.H. Wielers, B.P.J. Joghi, J. Van Beijnum, M. De Boer, M. Versluijs-Helder, J.W. Geus, J. Catal. 131 (1991) 178–189.
[58] X. Li, X. Lan, T. Wang, Green Chem. 18 (2016) 638–642.
[59] J.G. Dickinson, P.E. Savage, ACS Catal. 4 (2014) 2605–2615.
[60] J.-H. Lin, P. Biswas, V.V. Guliants, S. Misture, Appl. Catal. A: Gen. 387 (2010) 87–94.
[61] Z. Huang, F. Cui, J. Xue, J. Zuo, J. Chen, C. Xia, J. Phys. Chem. C 114 (2010) 16104–16113.
[62] C. Guimon, A. Auroux, E. Romero, A. Monzon, Appl. Catal. A: Gen. 251 (2003) 199–214.
[63] A.R. Naghash, T.H. Etsell, S. Xu, Chem. Mater. 18 (2006) 2480–2488.
[64] L.-F. Chen, P.-J. Guo, M.-H. Qiao, S.-R. Yan, H.-X. Li, W. Shen, H.-L. Xu, K.-N. Fan, J. Catal. 257 (2008) 172–180.
[65] Z. Huang, H. Liu, F. Cui, J. Zuo, J. Chen, C. Xia, Catal. Today 234 (2014) 223–232.
[66] Y. Shen, A.C. Lua, Appl. Catal. B: Environ. 164 (2015) 61–69.
[67] T. Yamauchi, Y. Tsukahara, T. Sakata, H. Mori, T. Yanagida, T. Kawai, Y. Wada, Nanoscale 2 (2010) 515–523.
[68] J.-H. Lin, V.V. Guliants, ChemCatChem 4 (2012) 1611–1621.
[69] S.L. Pirard, J.G. Mahy, J.-P. Pirard, B. Heinrichs, L. Raskinet, S.D. Lambert, Microporous Mesoporous Mater. 209 (2015) 197–207.
[70] Q. Wang, X.Y. Wang, J.L. Liu, Y.H. Yang, J. Nanopart. Res. 19 (2017) 25.
[71] R. Ferrando, J. Jellinek, R.L. Johnston, Chem. Rev. 108 (2008) 845–910.
[72] A. Jha, D.-W. Jeong, J.-O. Shim, W.-J. Jang, Y.-L. Lee, C.V. Rode, H.-S. Roh, Catal. Sci. Technol. 5 (2015) 2752–2760.
[73] Z.-H. Lu, J. Li, G. Feng, Q. Yao, F. Zhang, R. Zhou, D. Tao, X. Chen, Z. Yu, Int. J. Hydrog. Energy 39 (2014) 13389–13395.
[74] J. Luo, M. Monai, C. Wang, J.D. Lee, T. Duchon, F. Dvorak, V. Matolin, C.B. Murray, P. Fornasiero, R.J. Gorte, Catal. Sci. Technol. 7 (2017) 1735–1743.
[75] A. Jha, D.W. Jeong, J.O. Jang, Y.L. Lee, C.V. Rode, H.S. Roh, Catal. Sci. Technol. 5 (2015) 2752–2760.
[76] C.A. Ramírez-López, J.R. Ochoa-Gómez, M.a. Fernaíndez-Santos, O. Gómez-Jiménez-Aberasturi, A. Alonso-Vicario, J. s. Torrecilla-Soria, Ind. Eng. Chem. Res. 49 (2010) 6270–6278.